Al-Hinai M, Hassanien R, Watson SMD, Wright NG, Houlton A, Horrocks BR.
Metal-conductive polymer hybrid nanostructures: preparation and electrical properties of palladium-polyimidazole nanowires.
***Nanotechnology* 2016, 27(9): 095704.**

Metal-conductive polymer hybrid nanostructures: preparation and electrical properties of palladium-polyimidazole nanowires

Mariam Al-Hinai[1], Reda Hassanien*[2], Scott M. D. Watson[3], Nicholas G. Wright,[4] Andrew Houlton[3] and Benjamin R Horrocks[3]

[1] College of Applied Sciences Sohar, Engineering Department, P.O. Box 135, P.C. 311, Oman

[2] Department of Chemistry, Faculty of Science, Assiut University, New Valley Branch, El-Kharja 72511, Egypt.

[3] Chemical Nanoscience Laboratory, School of Chemistry, Bedson Building, Newcastle University, NE1 7RU, UK

[4] School of Electrical and Electronic Engineering, Merz Court, Newcastle University, NE1 7RU, UK

Abstract

A simple, convenient method for the formation of hybrid metal/conductive polymer nanostructures is described. Polyimidazole (PIm) has been templated on λ-DNA *via* oxidative polymerisation of imidazole using $FeCl_3$ to produce conductive PIm/DNA nanowires. The PIm/DNA nanowires were decorated with Pd (Pd/PIm/DNA) by electroless reduction of $PdCl_4^{2-}$ with $NaBH_4$ in the presence of PIm/DNA; the choice of imidazole was motivated by the potential Pd(II) binding site at the pyridinic N atom. The formation of PIm/DNA and the presence of metallic Pd on Pd/PIm/DNA nanowires were verified by FTIR, UV-Vis and XPS spectroscopy techniques. AFM studies show that the nanowires have diameters in the range 5–45 nm with a slightly greater mean diameter (17.1 ± 0.75 nm) for the Pd-decorated nanowires than the PIm/DNA nanowires (14.5 ± 0.89 nm). After incubation for 24h in the polymerisation solution, the PIm/DNA nanowires show a smooth, uniform morphology, which is retained after decoration with Pd. Using a combination of scanned conductance microscopy (SCM), conductive AFM and two-terminal measurements we show that both types of nanowire are conductive and that it is possible to discriminate different possible mechanisms of transport. The conductivity of the Pd/PIm/DNA nanowires, (0.1 - 1.4 S cm^{-1}), is comparable to the PIm/DNA nanowires (0.37 ± 0.029 S cm^{-1}). In addition, the conductance of Pd/PIm/DNA nanowires exhibits Arrhenius behaviour (E_a = 0.43 ± 0.02 eV) as a function of temperature in contrast to simple Pd/DNA nanowires. These results indicate that although the Pd crystallites on Pd/PIm/DNA nanowires decorate the PIm polymer, the major current pathway is through the polymer rather than the Pd.

* Corresponding author: reda.h@scinv.au.edu.eg

Introduction

Nanowires are of fundamental interest in investigations of nanoscale charge transport and are also studied for possible applications either as interconnects in microelectronics or as transducers in chemical sensors.[1-2] DNA-templated nanowires are a particular class of nanowires in which a conductive material is grown on a DNA template in order to direct the growth of the material into the form of a long, thin nanowire.[3-6] DNA is a material of choice in these processes because it is chemically robust, long and has specific recognition and self-assembly properties.[5] DNA has already been shown to be a template for the directed growth of metals,[6-11] semiconductor nanoparticles[12,13] and conductive polymers.[14-20]

The intrinsic electrical conductivity of DNA molecules is poor, therefore it is necessary to form electronically conductive materials on the DNA[6,7,21] or to make chemical modifications of the DNA,[22-24] to enhance the conductivity. Metals, including Pd, can be readily assembled on DNA *via* the chemical or photoinduced reduction of DNA-complexed metal ions.[10,25-27] Electronic transport measurements have been made with DNA-templated metal wires and the results demonstrate that they may be used in electronic circuits and sensors.[6,7] However, the growth of metals on DNA does not always lead to smooth structures; objects with dendritic morphologies are common.

We previously reported the preparation and the electrical properties of polypyrrole, polyindole and poly(2,5-(bis-2-thienyl)-pyrrole) upon DNA templates.[16,18,19] Oxidative polymerisation in DNA-containing solutions resulted in thin, homogeneous and uniform nanowires because the cationic oligomers are strongly attracted to the anionic sugar–phosphate backbone of DNA molecules.[16] Compared to DNA-templated metals, the polymer nanowires typically show a rather smooth morphology. A coarse-grained thermodynamic approach suggests that the low surface tension of polymers (relative to metals) favours the formation of smooth nanowires. Polymers can therefore be used to introduce additional functionality to the nanowires by a suitable choice of monomer, in particular by providing metal-binding sites such as alkynyl groups for Ag(I).[21]

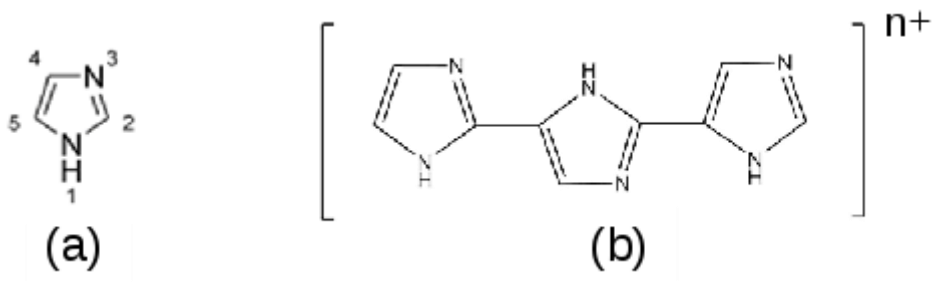

Scheme 1. (a) Imidazole and (b) poly(imidazole). Oxidative polymerisation is thought to occur via the C2 and C5 positions. This leaves the N3 available for metal binding.

Despite the importance of the imidazole ring in biological systems[28] and as a ligand for metal ions,[29] polyimidazole (PIm, Scheme 1b) has received less attention than conjugated polymers of the other five-membered ring heterocycles such as pyrrole and thiophene. Previous investigations of bulk polyimidazole (PIm) have reported conflicting values of the electronic conductivity. Wang and co-workers synthesised PIm and four of its derivatives by electrochemical and chemical polymerisation and found that none of these products exhibited electrical conductivity.[30] However, Raj and co-workers reported a conductivity of 1.9×10^{-3} S cm^{-1}.[31]

In this work, we describe the preparation and characterization of a novel hybrid metal/polymer nanowire comprising a polyimidazole core and a palladium shell. DNA-templated polyimidazole nanowires (PIm/DNA) are formed first and subsequently used to nucleate the growth of a Pd coating on the polymer nanowire (Pd/PIm/DNA). The choice of polyimidazole is motivated by the extra nitrogen atom (N3; Scheme 1a) compared to polypyrrole, which may act as a ligand to bind Pd.[32,33] The choice of palladium is motivated by the fact that this metal is known to form relatively smooth DNA-templated nanowires with which the electrical properties of the hybrid can be compared.[27] The nanowires are first characterised chemically (FTIR, XPS) and structurally (AFM, SEM). We then show that it is possible to discriminate between different charge transport pathways in such a structure using a range of probe microscopy and two-terminal I-V characterisation techniques to investigate the electronic conductivity of these nanowires.

Experimental

Materials

Lambda DNA (*λ*-DNA, 500 ng μL^{-1}) with a length of 17 μm (48 kbp) was purchased from New England Biolabs, cat no. N30011S (New England Biolabs (U.K.) Ltd. Hitchin, Herts. SG4 0TY United Kingdom). Imidazole, ferric chloride, calf thymus DNA (highly polymerised, 6% sodium) and other chemicals were purchased from Sigma-Aldrich. If not stated otherwise, all solutions were prepared in water from a Barnstead Nanopure^{TM} purification train with nominal resistivity of 18.2 MΩ cm. Si wafers were obtained from Compart Technology, Cambridge, UK as either n-Si(111)/SiO_2 (for AFM & EFM) or p-Si (100) (for FTIR). Detailed specifications are given below. Si wafers were degreased in acetone and cleaned by oxidation in piranha solution (4:1 concentrated sulfuric acid : 30 vol hydrogen peroxide).

Methods

Preparation of bulk PIm.

Prior to preparing poly(imidazole) (denoted PIm) in solutions containing λ-DNA, bulk PIm was prepared separately as a control for FTIR experiments. This was done by adding an aqueous $FeCl_3$ solution (0.2M) to an aqueous imidazole solution (0.1M) in a 2:1 mole ratio. On stirring, the colour changed to dark brown and the solution became viscous. After standing overnight, the polymer was purified by dialysis to remove traces of Fe salts and then collected on a rotary evaporator and left in vacuum overnight to dry. The PIm was then characterised using FTIR spectroscopy (using a KBr pellet technique).

Formation of PIm/DNA nanowires. PIm/DNA nanowires were chemically synthesized using $FeCl_3$ as an oxidant at room temperature. In a typical synthesis, 5 μL of freshly prepared imidazole solution (1 mM) was added to 20 μL of *λ*-DNA (500 ng μL^{-1}) in the presence of 5 μL of $MgCl_2$ (0.5 mM), then 5 μL of $FeCl_3$ (1 mM) was added drop-wise into this solution. This is the solution referred to as PIm/DNA solution below.

Formation of Pd/PIm/DNA and Pd/DNA nanowires. To PIm/DNA solution, prepared as described above and incubated at room temperature for 24h unless otherwise indicated, 4 μL K_2PdCl_4 (3 mM) was added and stirred at room temperature to allow Pd(II) to bind to the imidazole. After allowing the reaction mixture to stand at room temperature for 10 min, 4 μL $NaBH_4$ (10 mM) solution was added to previously prepared solution to reduce the Pd(II) ions. The solution was thoroughly mixed and allowed to react for at least 1h at room temperature prior to analysis. In some experiments (UV/Vis spectroscopy), larger volumes were required. In those cases, calf thymus DNA and slightly different concentrations of monomer/metal were used. Details are given alongside the description of the UV-Vis measurements below. Pd/DNA was prepared in the same way as Pd/PIm/DNA, but using λ-DNA instead of PIm/DNA on which to carry out the electroless deposition of Pd, as previously reported.[27]

Deposition of Pd/PIm/DNA nanowires on substrates for microscopy. In order to facilitate the alignment of individual nanowires on Si/SiO_2 substrates, the hydrophobicity of the SiO_2 was increased by treating the Si/SiO_2 substrates with chlorotrimethylsilane (Me_3SiCl) vapor for about 10 min. The silanization reduces the number of adhering nanowires and allows them to be 'combed' – that is aligned and extended by the surface forces produced as a droplet of nanowire solution is dragged across the surface by a pipette tip.[34] Typically, 2–3 µL (Pd)/PIm/DNA solution was dropped onto the Si/SiO_2 surface and combed; the remaining solution was removed with a micropipette and/or wicking with filter paper.

Deposition of Pd/PIm/DNA nanowire networks on substrates for two-terminal electrical characterisation. In some experiments (Fig. 10 below), networks of nanowires rather than individual nanowires were desired; in these cases the silanization was omitted and large numbers of nanowires adhered to the substrate directly from a 2–3 µL droplet of (Pd)/PIm/DNA solution without combing.

Fourier transform infrared spectroscopy. Transmission FTIR spectra in the range 600–4000 cm^{-1} were recorded with a Bio-Rad Excalibur FTS-40 spectrometer (Varian Inc., Palo Alto, CA) equipped with a liquid-nitrogen-cooled MCT detector. 128 scans were co-added and averaged and the resolution was 4 cm^{-1}. The DNA and PIm/DNA

samples were prepared by drop-casting aqueous solutions (8 μL) on pirhana-treated p-type Si(100) substrates (<100> oriented; 525 μm thickness, boron-doped, *p*-type, 5-15 Ohm cm resistivity). Drop-cast solutions were left to dry for 1h prior to analysis. A clean Si(100) chip served as the background.

X-ray Photoelectron Spectroscopy. A Kratos Axis Ultra 165 photoelectron spectrometer equipped with a monochromic Al K- X-ray excitation source (1486.7 eV) with an operating power of 150 W (15 kV, 10 mA) was used to collect photoemission spectra of PIm/DNA and Pd/Pim/DNA samples. The chamber pressure was 3.2 x 10^9 Torr. The photoelectrons were filtered by the hemispherical analyzer and recorded by multichannel detectors. For the survey scan, the pass energy was 20 eV and the step size was 0.3 eV. Some higher resolution spectra were recorded with a pass energy of 5 eV and a step size of 0.1 eV. The binding energies obtained in the XPS analysis were calibrated using Au_{4f} as a reference. Spectral peaks were fitted with mixed singlet functions or a Doniach–Sunjic doublet function after subtraction of a Shirley-type background[35] using the WinSpec program developed by LISE laboratory, Universitaires Notre-Dame de la Paix, Namur, Belgium. PIm/DNA samples were prepared for XPS by depositing 5 μL of solution on a clean Si(100) substrate and then left to dry in air at room temperature in a laminar flow hood to minimize contamination (Model VLF 4B, Envair, Haslingden, Lancs, U.K.) before being inserted into the chamber.

Preparation of substrates for AFM studies. For AFM analysis of topography, n-doped Si <111> wafers were used. Electrical characterisation by EFM and c-AFM was carried out on Si/SiO_2 substrates. The wafers were cut into small pieces (1.0 cm x 1.0 cm) with a diamond tip pen, then sequentially cleaned using a cotton bud soaked in acetone, propanol and finally water, and treated with “piranha” solution (4:1 H_2SO_4/H_2O_2) for 45 min. This provides a highly hydrophilic surfaces rich in OH-termini which was rinsed in water and dried in an oven for 15 minutes at 50 ºC. In order to obtain a hydrophobic surface the Si substrate was treated with a vapour of TMS by placing the surface (polished side facing up) on the top of a specimen bottle containing 100 µL of Me_3SiCl for 10 min. Static contact angle measurements of the substrate before and after TMS-modification were carried out using a CAM100 system (KSV

Instruments Ltd., Helsinki, Finland). The contact angle before TMS treatment was < 5° and measurements after treatment with TMS for 10 min typically gave contact angles between 60° and 70°. Wetting measurements were performed using Cam-100 contact angle meter (KSV Instruments Ltd. Helsinki, Finland) using deionized water as a solvent. Mean contact angle was determined by the included software (using a Young-Laplace method) via the mounted high resolution camera.

Probe and electron microscopy – topography and electrical characterisation of single nanowires. All of the atomic force microscopy (AFM) imaging was performed in tapping mode^{TM} in air on a Dimension Nanoscope V (Veeco Inc., Metrology group) using NanoProbe tips (Veeco Inc.). All of the AFM images are height images unless otherwise indicated. Vibrational noise was reduced with an isolation system (TMC, Peabody, MA, USA). Samples for AFM or scanning electron microscopy (SEM) were prepared by allowing 2-3 µL of PIm/DNA or Pd/PIm/DNA solution to dry on 1 cm^2 SiO_2/Si substrates at room temperature for 1h. The SiO_2 thickness was about 220 nm, as determined by a spectrometric thin film analyzer (Filmetrics F40).

For EFM and conductive AFM (c-AFM) measurements, we used MESP probes (n doped Si cantilevers, with a Co/Cr coating, Veeco Inc.). These probes are 200-250 µm long, with a resonant frequency of about 79 kHz, a quality factor (Q) between 200 and 260, and a spring constant between 1 and 5 N m^{-1}. For c-AFM measurements, a constant bias was also applied between the tip and the sample (the tip was grounded). Electrical contact was made by applying a drop of In/Ga eutectic to one corner of the chip and to the metallic chuck. c-AFM imaging was performed in contact mode, with an applied bias of 0.5 V. The imaged area was about 1 mm away from the In/Ga contact. The closed loop system of the Dimension V instrument makes it possible to reproducibly position the tip at a point of interest identified in the image of the PIm/DNA nanowire and to record current-voltage (I-V) measurements of a single nanowire at that point. The resistance was estimated from the reciprocal of the slope of the I-V curve at zero bias.

Lithography - microelectrode fabrication. Electrode structures were fabricated on n+-doped silicon wafers with a 300 nm thick insulating oxide layer using a standard image reversal photolithographic process (Scheme 2). Gold (Au) microelectrodes have

been fabricated to investigate the electrical characteristics of the polymer nanowires. This method of fabricating Au electrodes was adapted from our previous work.[18] First, an appropriate mask was prepared with four sets of large contact pads and small fingers and patterned using an image reversal photolithography process on the clean substrate. Next, reactive ion etching was used to make a 100 nm deep trench in a 220 nm thick SiO_2 dielectric. The trench was filled with e-beam-evaporated metals (10 nm Cr adhesion layer followed by 90 nm Au). This technique produces electrodes with a much reduced step height (5 – 10 nm, supporting information) at the boundary between the Au electrodes and the oxide gap in the final device and facilitates alignment of polymer nanowires across the gap. Next, a lift-off process was used to remove unwanted Cr and Au. The electrode design (Scheme 2) consisted of four identical patterns of crossed Au fingers attached to larger contact pads: the Au fingers were of width ~2 μm and length ~12 μm connected to rectangular Au pads fabricated on the same chip. The gap between neighbouring fingers was about 4 μm (AFM image provided in supporting information). The Au fingers in each cross provided contacts to the DNA-templated nanowires, and the large Au pads served as electrical contacts for external measurement of the system by a probe station.

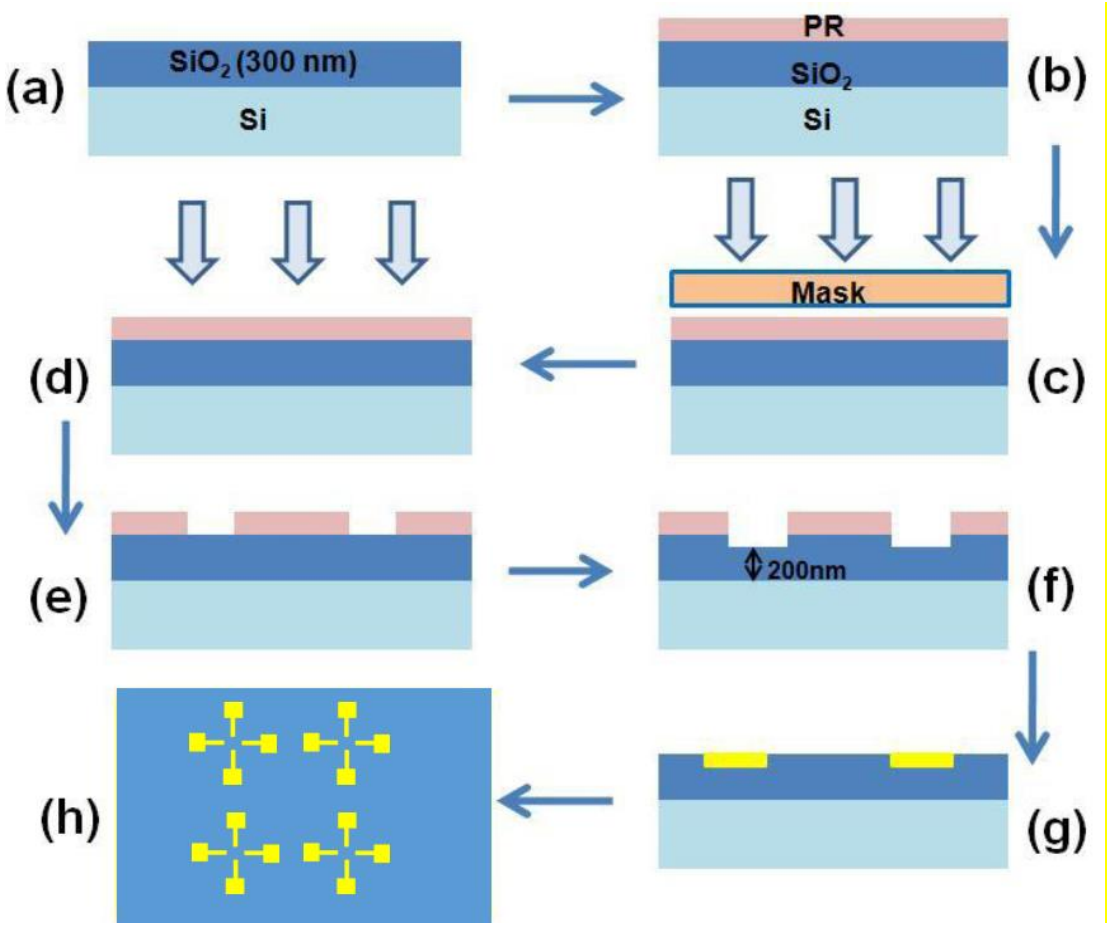

Scheme 2. Diagram of the photolithography process used to fabricate Au microelectrodes. **(a)** Clean Si/SiO_2 wafer. **(b)** Photoresist coating on the substrate. **(c)** Exposure with mask. **(d)** Plain exposure. **(e)** After developing. **(f)** After reactive ion etching. **(g)** After metal deposition. **(h)** Schematic of the electrode design showing the thin Au fingers and rectangular Au contact pads.

Two-terminal current-voltage measurements of nanowire networks. Two-terminal conductivity measurements of networks of Pd/PIm/DNA nanowires to compare with previous Pd/DNA networks were performed using the Au microelectrodes described above. Pd/PIm/DNA nanowires were deposited across the Au electrodes by drop-casting. As we have previously reported in the case of Pd/DNA nanowires, this procedure results in a network of nanowires if the oxide surface of the chip is left hydrophilic and not silanised.[27] Electrical measurements were made using a probing station (Cascade Microtech) and a B1500A semiconductor analyzer (Agilent). For each of the electrical tests, the current was measured for applied voltages from -10 to 10 V in steps of 0.05 V. All of the electrical measurements were carried out under dry nitrogen in the absence of illumination. I-V curves at various temperatures were

obtained on the probe station by controlling the sample temperature using a thermal chuck system (Model ETC-200 L, ESPEC, Japan).

Results and Discussion

First we use a combination of FTIR and X-ray photoelectron spectroscopy to demonstrate the formation of poly(imidazole) and Pd on the molecular DNA templates. Throughout the text PIm denotes poly(imidazole) prepared as a powder, PIm/DNA denotes poly(imidazole) prepared in nanowire form on a DNA template and PIn/DNA is the corresponding notation for a poly(indole) nanowire templated on DNA. Pd/PIm/DNA denotes a material which comprises Pd deposited on a PIm/DNA nanowire. Next, we characterise the structural properties of the PIm/DNA and Pd/PIm/DNA nanowires, principally their diameters, using AFM and electron microscopy. Finally, we investigate and compare the conductivity of the PIm/DNA and Pd/PIm/DNA nanowires using SCM, c-AFM and two-terminal I-V measurements as a function of temperature.

Fourier transform infrared spectroscopy

The FTIR spectra of bare DNA, imidazole monomer, PIm, PIm/DNA and the difference spectrum (PIm/DNA) - DNA are shown in Fig. 1. Additional FTIR and UV-Vis spectroscopic data is provided in the supporting information. The structure of PIm is more complex than polypyrrole (PPy), because a number of different coupling schemes are possible involving C-C or N-N linkages.[30] We cannot determine the precise coupling in our PIm/DNA nanowires from FTIR data, however it is possible to demonstrate an intimate association of the polymer with the DNA. In the DNA and PIm/DNA spectra, broad bands due to bound water in DNA are present, with maxima at 3332 and 3278 cm^{-1} respectively, although the negative feature in the difference spectrum (PIm/DNA)-DNA at 3300 cm^{-1} suggests that some water has been displaced upon interaction of PIm with DNA.[16] This effect is even more pronounced for Pd/PIm/DNA. The presence of DNA in the PIm/DNA and Pd/PIm/DNA is revealed clearly in the 800-1800 cm^{-1} region, especially in the bands around 1600-1700 cm^{-1} and 1100-1200 cm-1.[36-38] The spectra of both DNA itself and PIm/DNA and Pd/PIm/DNA are similar in this region, though a careful examination of the fingerprint region reveals that some of the DNA-related bands are slightly shifted relative to the

pure DNA spectrum (Supporting information). In particular, the P-O stretching modes in the region 1100-1200 cm^{-1} are split and shifted to higher energy.

In summary, the FTIR spectra indicate that the PIm-DNA sample is not a simple mixture of DNA and PIm but rather an intimate interaction of DNA with PIm in the hybrid polymer in a similar manner to our previous report for polymer/DNA nanowires.[16,18]

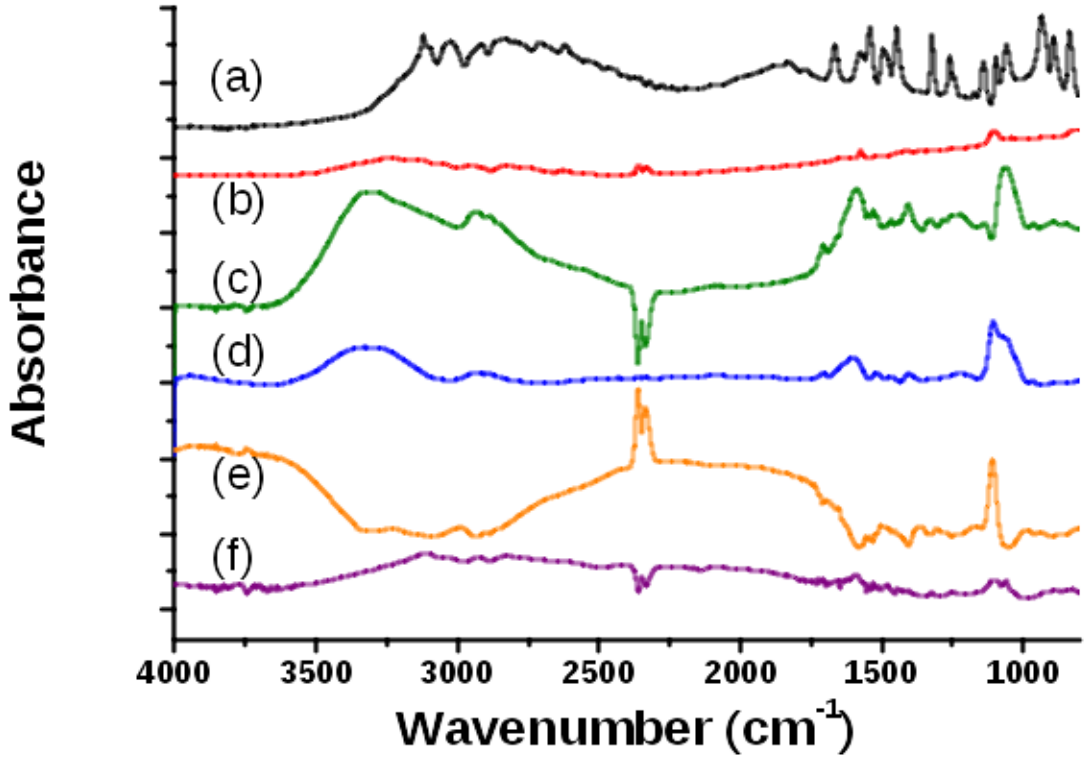

Figure 1. Transmission FTIR spectra of **(a)** imidazole (black); **(b)** bulk PIm (red); **(c)** DNA (green); **(d)** PIm/DNA (blue); **(e)** Difference spectrum (d)-(c) (orange) and **(f)** Pd/PIm/DNA (purple) in the 4000-800 cm^{-1} region. 128 scans were co-added and averaged and the resolution was 4 cm^{-1}. All spectra were recorded in air and the sharp feature which appears at 2360 cm^{-1} is a CO_2 miscancellation.

X-ray photoelectron spectroscopy

Fig. 2 presents core-level C_{1s}, N_{1s} and Pd_{3d} photoemission spectra for Pd/PIm/DNA. The survey spectrum (supporting information) of the Pd/PIm/DNA sample contains the characteristic peaks of the elements C, N due to the PIm and DNA templates, O, P due to the DNA templates and Pd in addition to the Cl derived from K_2PdCl_4 or $FeCl_3$ which is used as the oxidant in the polymerisation of imidazole. The P_{2p} peak at 132.1 eV, corresponds to the phosphate group of DNA.

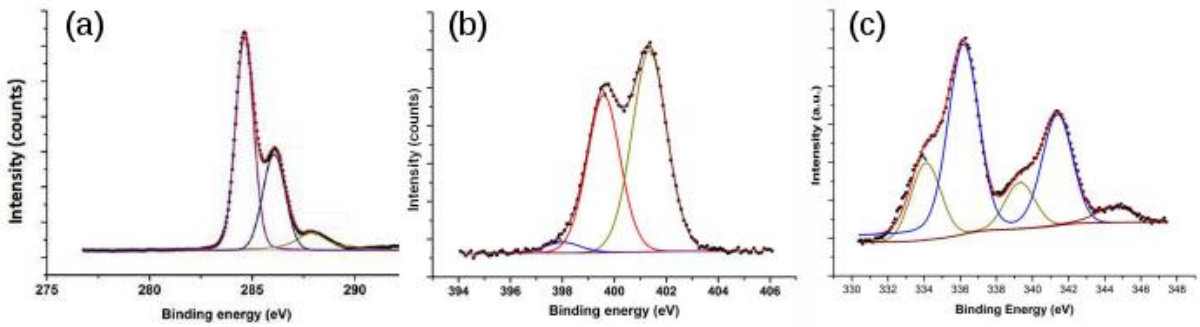

Figure 2: XPS spectra of Pd/PIm/DNA nanowires. **(a)** C_{1s} spectrum; **(b)** N_{1s} spectrum and **(c)** Pd_{3d} spectrum.

The C_{1s} spectrum of Pd/PIm/DNA nanowires (Fig. 2a) can be resolved into three different components centred at 284.6, 286.1 and 287.9 eV. Previous workers[39] have observed four components of DNA alone at 284.6, 286.5, 287.9 and 289.1 eV. The components at 284.6 and 286.1eV of the C_{1s} spectrum of Pd/PIm/DNA nanowires are assigned to C-H, C-C, and C-N species from PIm and DNA. The peak at 286.1 eV is more intense in the Pd/PIm/DNA spectrum than in pure DNA which reflects the contribution of the PIm in the sample. The peak at 287.9 eV may be attributed to the functional groups of the type, C═N or $C-N^+$, mainly from PIm, because this feature is also more intense in the Pd/PIm/DNA sample than its counterpart in the pure DNA spectrum.[39]

Fig. 2b shows the N_{1s} spectrum of Pd/PIm/DNA nanowires, it comprises three components; two main components at 399.6 eV and 401.4 eV and a small peak at a lower binding energy of 398.0 eV. Previous workers have observed two components in the N_{1s} spectra of DNA; at 398.8 eV and another at 400.6 eV which is assigned to the pyrimidine N atoms.[39] The shift to larger binding energies in the Pd/PIm/DNA spectrum (Fig. 2b) indicates the contribution from the N atoms of PIm to these features. We assign the higher peak at 401.4 eV to charged nitrogen atoms in PIm. This is consistent with previous reports on polyindole[40] and polypyrrole.[41] The third feature at 398.0 eV is definitely not present in the N_{1s} spectrum of pure DNA and can be assigned to PIm alone.

The XPS spectrum of the Pd/Pim/DNA sample in the Pd_{3d} region (Fig. 2c) clearly shows that there are two Pd oxidation states. Two peaks were detected at 336.2 eV for $Pd_{3d5/2}$ and at 341.5 eV for $Pd_{3d3/2}$ and these peaks represent imidazole-bound

Pd(II). Two smaller peaks can also be observed at 334.1 eV for $Pd_{3d5/2}$ and 339.4 eV $Pd_{3d3/2}$ are attributed to Pd^0. These binding energies are in agreement with results reported for Pd^0 and Pd(II)[42-44] and confirm the formation of metallic palladium, but also the presence of substantial unreduced Pd(II). The extra peak at 344.5 eV is attributed to surface plasmon energy loss[45] associated with the $Pd_{3d5/2}$ electrons of binding energy 334.1 eV; the corresponding energy loss associated with $Pd_{3d3/2}$ is out of the measured energy range. The observed plasmon energy (10.4 eV) is larger than expected (~7 eV) for a Pd surface plasmon,[46] but this has also been observed for Pd/DNA nanowires.[27]

Overall, the XPS data for Pd/PIm/DNA samples clearly demonstrate the formation of a Pd coating on the poly(imidzaole). The spectra are similar to those reported for Pd/DNA nanowires,[27] but with two notable differences: (i) the N_{1s} spectrum reveals the presence of imidazole nitrogen atoms and (ii) the plasmon loss energy is 10.4 eV for Pd/PIm/DNA compared to 11.2 eV for Pd/DNA. This is may be a result of the differences in the Pd surface chemistry in the two systems.

AFM characterisation of aligned PIm/DNA and Pd/PIm/DNA nanowires

AFM images of PIm/DNA samples show the formation of PIm along DNA strands (Fig. 3). By comparing the heights of the wires appearing in Fig. 3a, which were aligned by molecular combing after ~2 hours of incubation, it is clear that the polymer is beginning to coat the DNA molecules, but some uncoated DNA strands remain and there is also globular material associated with the DNA. Such features are typical for the early stages of conductive polymer templating on DNA.[20] Non-templated material was also often observed; this is most likely either polymer or residual buffer salts.[47]

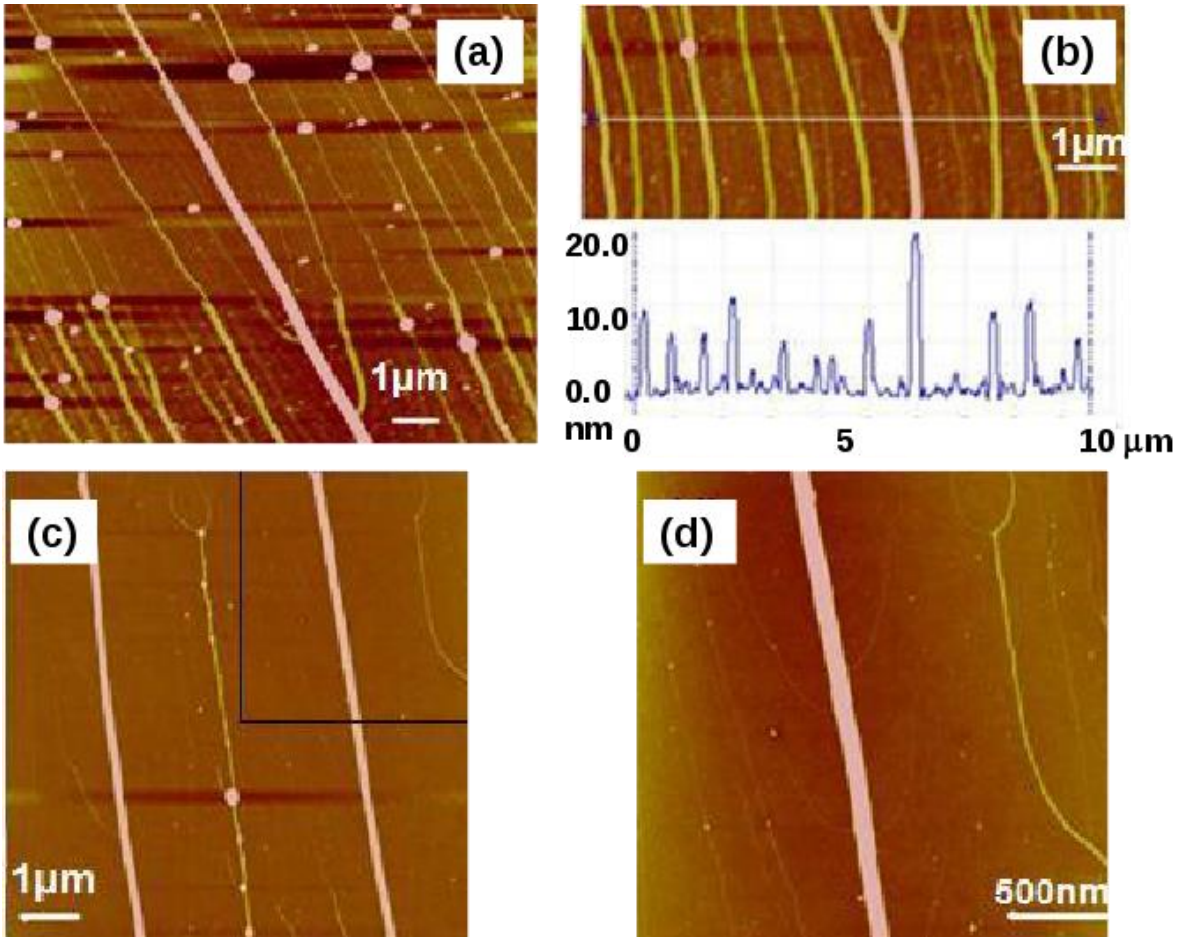

Figure 3: AFM images of PIm/DNA nanowires aligned on Si/SiO_2 substrate **(a)** After 2 hours of incubation, showing uncovered parts of DNA with the polymer. **(b)** Upper, image: after 24 hours of incubation; lower, height profile: section along the white horizontal line drawn across the middle of image (b) showing nanowires with heights 3 - 20 nm. **(c)** Parallel, smooth nanowires **(d)** zoomed image of the nanowires in the upper right corner of (c). The grayscale in all images corresponds to a height range of 35 nm.

After 24 hours of incubation, polymer-coated DNA nanowires were observed showing a range of diameters, but most of the individual nanowires are relatively uniform along their length (Fig. 3b). A comparison with Pd/PIm/DNA smoothness is made below. The distribution of diameters can be attributed to different thicknesses of the PIm coating, however there is also evidence of “rope” formation as can be observed in the branching at the top of the image of the thickest nanowire near the middle of Fig. 3b as well as the leftmost nanowire of Fig. 3c and the thick nanowire in Fig. 3d. Such ropes have been observed previously for polypyrrole/DNA nanowires and correspond to multiple DNA-templated polymer strands winding around each other.[17]

Fig. 4a illustrates the topography of the nanowires after metallisation with Pd. The smooth, relatively uniform, morphology of the PIm/DNA nanowires is retained after

metallisation. Some non-templated particles are visible in Fig. 4a and 4c, which are assigned as residual salts. Although individual nanowires are uniform, there is substantial variation in diameter (height) between nanowires and we also observe some rope formation, e.g., the thick nanowire in the centre of Fig. 4c, as evidenced by the existence of branches along the main 'trunk' of the nanowire. Fig. 4b shows an SEM image of Pd/PIm/DNA drop-cast from solution onto a Si/SiO_2 chip. The individual nanowires appear stretched out around the periphery of the main mass (upper right of the image). We believe this is due to a kind of "molecular combing" as surface forces at the receding edge of the drying droplet of solution causes the nanowires to be aligned normal to the main mass. This effect is useful because it facilitates the characterization of individual nanowires by conductive AFM (c-AFM) below.[18,27]

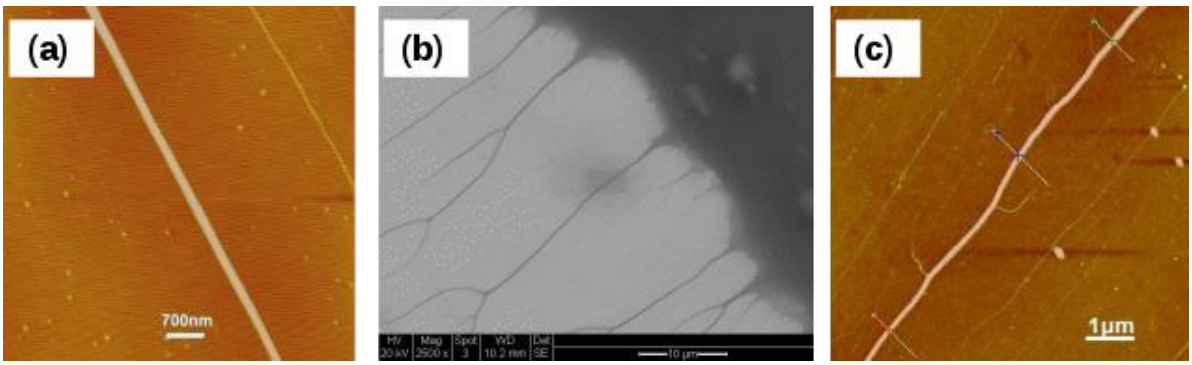

Figure 4: A selection of AFM images of Pd/PIm/DNA nanowires aligned on Si/SiO_2 substrates: **(a)** Pd-(PIm-DNA) nanowire of diameter 25 nm after 4 days of incubation (grayscale corresponds to a height range of 30 nm). **(b)** SEM image of drop-cast Pd/PIm-DNA nanowires. The scale bar is 10 μm. **(c)** Example of a Pd/PIm/DNA nanowire which shows evidence of rope formation (grayscale corresponds to a height range of 35 nm).

In order to explore the variations in thickness between nanowires discussed above, about 100 nanowires of both PIm/DNA and Pd/PIm/DNA were imaged and the histogram of the heights (= diameters) of these nanowires are shown in Figs. 5a and 5b respectively. The diameter for each individual nanowire was obtained by averaging along a 5 µm continuous length of the nanowire. The percentage of nanowires with thicknesses greater than 10 nm is higher in the case of Pd/PIm/DNA which is expected upon metallisation of the PIm/DNA nanowires. The overall height range (5-45 nm) of the Pd/PIm/DNA nanowires is comparable with previous Pd/DNA nanowires.[27]

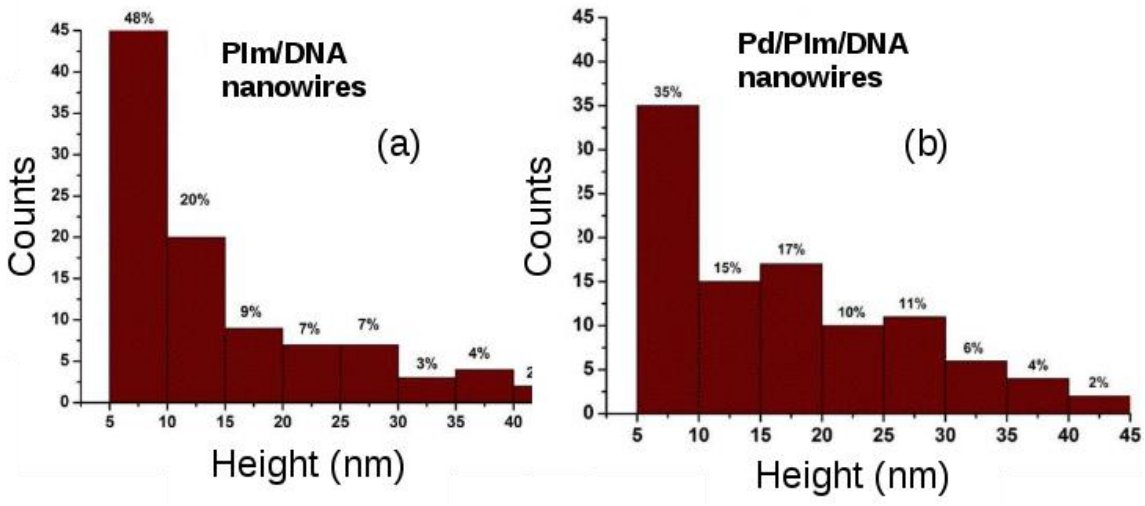

Figure 5: Histograms of the distribution of the nanowires heights of **(a)** PIm/DNA, mean ± standard deviation of diameter = 14.5 ± 0.89 and **(b)** Pd/PIm/DNA, mean ± standard deviation of diameter = 17.1 ± 0.75 nm. The statistics were compiled from images of 100 nanowires for each type of nanowire after 24h incubation.

To make a quantitative comparison of smoothness/uniformity, the standard deviation of Pd/DNA[48] and Pd/PIm/DNA nanowire diameters along 5 μm lengths of nanowires, at 5 evenly spaced intervals, was calculated from AFM images. For each nanowire, the fractional standard deviation for each nanowire was computed by dividing the standard deviation by the mean diameter. This process was repeated for 10 nanowires of each type and we report the mean and the standard error of the fractional standard deviation along a nanowire as our measure of uniformity. The wires analysed were chosen to reflect the range of sizes observed - mean diameter ~20 nm for both, range 7-35 nm for Pd/DNA and 10-30 nm for Pd/PIm/DNA. A fractional standard deviation of (0.076 ± 0.005) was obtained for Pd/DNA nanowires and for Pd/PIm/DNA a larger value of (0.76 ± 0.24) was found. These results contrast with the previously reported case of Ag templated on DNA versus Ag templated on a poly(alkynyl-thienylpyrrole)/DNA template; Ag/PTp/DNA nanowires were observed to be more smooth than simple Ag/DNA nanowires.[21] Two effects are important: (i) the growth of Pd NPs in these 1D structures is known to be very different to that of other metals such as Ag and (ii) the PIm/DNA nanowires themselves show numerous branches. Ag forms on a DNA template as a series of crystals in a beads-on-a-string morphology that eventually overlap, but on the poly(alkynyl-thienylpyrrole)/DNA template the Ag forms as very small crystallites and so the nanowire appears smooth to the AFM.[21] Instead Pd forms as very small crystallites on bare DNA also and therefore there is no change in growth morphology on a PIm/DNA template comparable to the case of Ag.

The fractional standard deviation of 0.76 for Pd/PIm/DNA indicates a substantial variation in diameter along each nanowire, but this is mainly due to the presence of many branches (seen in Fig. 3a for PIm/DNA and Fig. 4c for Pd/PIm/DNA).

Electrical characterisation of nanowires using scanning conductance microscopy (SCM)

Electric force microscopy (EFM) operated in the mode known as scanned conductance microscopy (SCM) provides a useful contactless tool for qualitative testing of the conductivity of a single nanowire prior to any quantitative measurement of its conductivity.[49] The method is based on the storage of energy in the tip/nanowire/substrate capacitor and the nanowire conductance influences the measurement via the RC time constant for polarisation of the nanowire. For SCM studies, the nanowires are aligned on Si/SiO_2 chips with an oxide thickness ~200 nm and the phase shift between the driving force and the tip motion is recorded as a function of applied dc bias (V) as the tip crosses above the nanowire at a constant lift height (typ. 50-100 nm). As shown by Staii and co-workers,[50] a negative phase shift with a V^2 applied bias dependence is an indication of a conductive nanowire. Objects which are merely polarisable and do not have charges which can move away from the vicinity of the tip produce a positive phase shift. The SCM was used to test the conductivity of both PIm/DNA and Pd/PIm/DNA nanowires.

SCM phase data for PIm/DNA and Pd/PIm/DNA nanowires (Fig. 6a and Fig. 6b) shows the expected parabolic dependence of the phase shift on bias for voltages between -10 and +10 V with only slight asymmetry between negative and positive bias (Fig. 6a, & Fig. 6b). This indicates that the data observed are mainly due to the conductance effect and the effect of the trapped charges (which produces a term linear in the dc bias) may be ignored. It is also clear that the phase shift is decreased by increasing the lift height which is consistent with the model.[50] Figs. 6(a1-a4) & 6(b1-b4) show selections of scanned conductance images with their associated height images and an example of a section profile across a nanowire of the observed phase shift. The nanowires appear as dark lines in the scanned conductance images; this corresponds to a negative phase shift as the tip crosses the nanowire and demonstrates the existence of free charges in the nanowire.

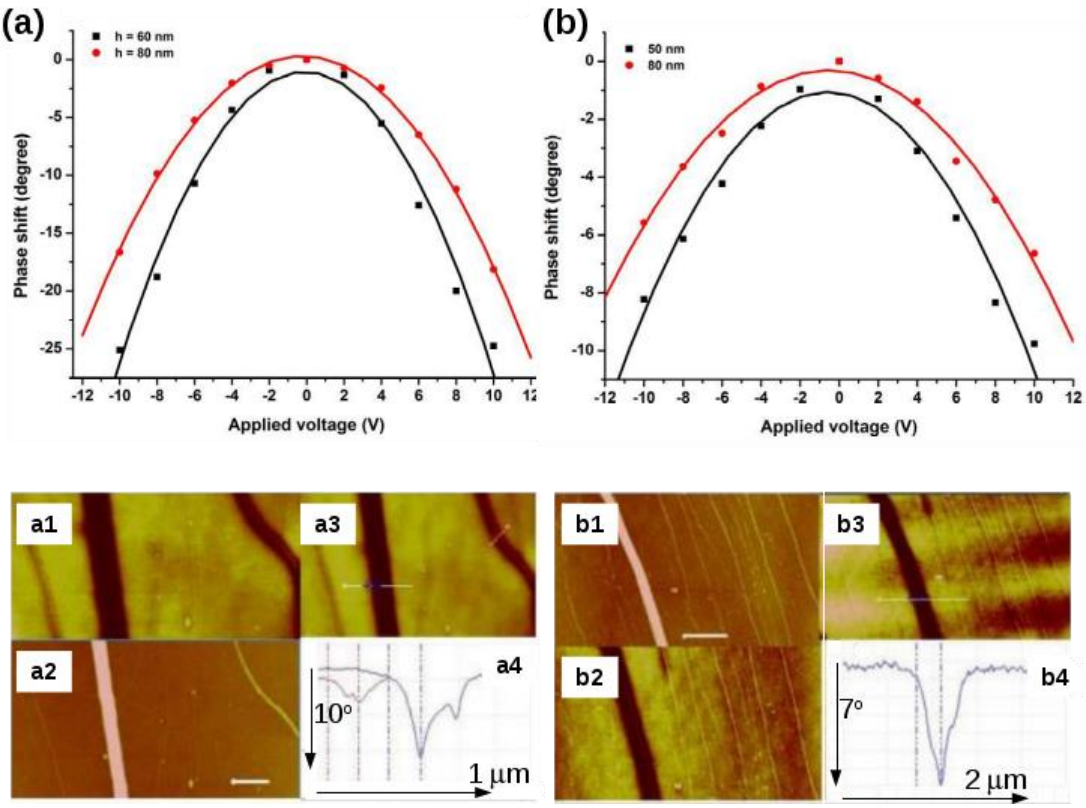

Figure 6: **(a)** SCM phase against applied dc bias for a 30 nm diameter PIm/DNA nanowire aligned on a SiO_2/Si surface with an SiO_2 thickness of 220 nm. Two datasets are shown for lift heights 60 and 80 nm respectively. **(a1, a3)** SCM phase images of PIm/DNA nanowires of diameters of 35nm and 7nm at lift height 60nm and tip/sample bias of **(a1)** 6V and **(a3)** -6V. **(a2)** AFM height image of the nanowires in a1 & a3; the scale bar represents 500nm. **(a4)** A line section through the phase image (a3) of the two larger nanowires visible in (a3) at -6V.
(b) SCM phase against applied dc bias for a 25 nm diameter PIm/DNA nanowire aligned on a SiO_2/Si surface with an SiO_2 thickness of 220 nm. Two datasets are shown for lift heights 60 and 80 nm respectively. **(b1)** AFM height image of the nanowires in b2 & b3, the scale bar represents 500nm. **(b2, b3)** SCM phase images of a Pd/PIm/DNA nanowire of diameter 22 nm at a lift height of 60nm and tip/sample bias of **(b2)** 6V and **(b3)** -6V. **(b4)** A line section through the phase image (b3) of the large nanowire visible in (b3) at -6V.
In all phase images, the grayscale corresponds to 3 degrees. The cantilever spring constant (k) = 5 N m^{-1} and the quality factor (Q) =250.

The width of the phase images of the nanowires in Figs. 6a & 6b is enlarged compared to height AFM images because of the long-range nature of the interaction. The profile of the phase shift across the nanowire observed for PIm/DNA (Fig. 6a4) is a W-shape[51] typical for semiconducting and conjugated polymer materials.[50,52] This feature almost disappeared in the Pd/PIm/DNA nanowire phase images as shown in Fig. 6b4; this is similar to the case of Pd/DNA nanowires.[27] It is also worth noting that the phase images (Figs. 6b2 & 6b3 especially) show examples of bare DNA (thin lines to the right of the image, height < 2nm) which have a weak positive phase shift that is

characteristic of insulating objects as has also been reported for other polymer samples[18] and in DNA itself.[53]

A direct comparison between the SCM phase shifts for Pd/PIm/DNA and Pd/DNA nanowires (Fig. 7a & Fig. 7b) was made by keeping the lift height (60 nm) and SiO_2 thickness (220 nm) constant and by selecting nanowires of consistent diameter (25 nm). It is clear that the phase shifts for both Pd/DNA and Pd/PIm/DNA nanowires are comparable in the bias range from -10 to 10V (within about ± 0.25º). A slight asymmetry of the parabolic curve is also observed in Fig. 7a; this is typically due to the effect of trapped charge which produces a linear dependence on applied bias. Fig. 7b shows the effect of the nanowire diameter on the scanned conductance effect for both types of nanowires. The SCM effect was quantified by fitting a quadratic equation to the raw data (phase shift versus dc bias, *V*) for different nanowire diameters and for both cases. Then the best-fit coefficient of V^2 was plotted as a function of nanowire diameter.

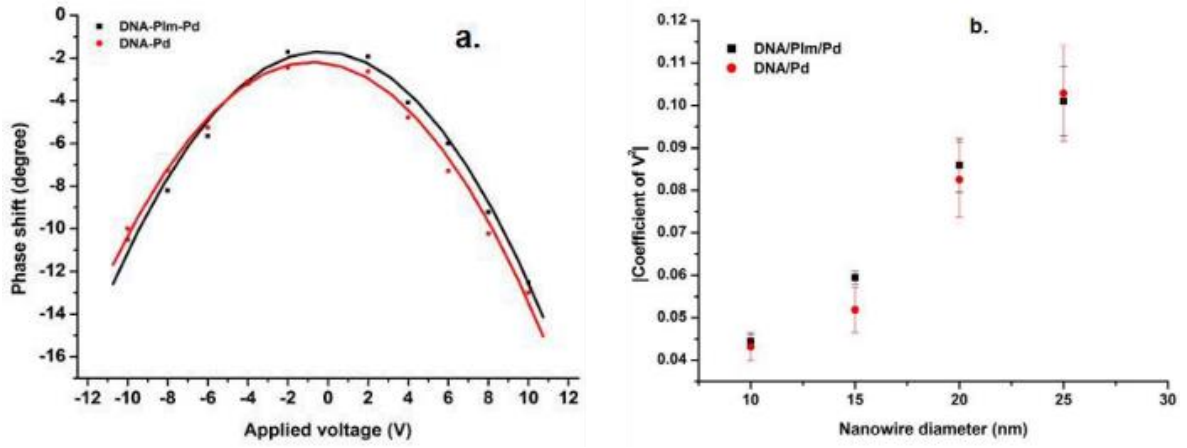

Figure 7: A comparison of the SCM measurements of Pd/DNA and Pd/PIm-DNA nanowires. **(a)** Phase shifts as a function of applied voltage of Pd/DNA and Pd/PIm/DNA nanowires of 25 nm diameter at lift height 60 nm. **(b)** Coefficient of V^2 from a quadratic fit of phase shift versus dc bias V for different nanowire diameters (for both Pd/DNA and Pd/PIm/DNA) against the nanowire diameter at a constant lift height 60 nm. The error bars are standard deviations computed from measurements on 5 nanowires of each diameter.

Fig. 7b shows that the phase shift increases with increasing nanowire diameter and the results are comparable for both types of nanowires. Similar observations for the phase shift versus diameter have also been observed for PIn/DNA.[18] In summary, SCM measurements show similarity in the phase shifts of both Pd/DNA and Pd/PIm-DNA nanowires. However, it should be noted that the SCM phase is independent of

the value of conductance if the nanowire is polarised on a timescale shorter than that of the AFM experiment. Further electrical characterisation was therefore carried out using c-AFM and two terminal I-V measurements to gain more quantitative insight into the electrical properties of these nanowires.

Measuring the conductivity of single nanowires using c-AFM

Conductive AFM (c-AFM) is a useful technique for measuring the conductance of a single nanowire and estimating its conductivity.[49] For this experiment the PIm/DNA and Pd/PIm/DNA nanowires were deposited on oxidised Si substrates to measure the electrical conductance of a single nanowire for both samples. The method used is the same as that employed for PIn/DNA nanowires.[18] One macroscopic contact using In/Ga eutectic is made to the large mass of nanowires produced by a dried droplet, e.g., that in the upper right of Fig. 4b. The metallised tip provides the second contact and its location may be adjusted along an individual nanowire at the droplet edge to allow determination of resistances for varying lengths of the nanowire. The resistances discussed below are all obtained from the slope of linear I-V characeristics at zero bias.

Fig. 8a shows the resistance values of a single PIm/DNA nanowire calculated from the *I-V* curves at different points on the nanowire (as shown in the corresponding current map of the nanowire in Fig. 8a (inset). The resistance is plotted as a function of relative distance from the contact point. It is clear that the resistance increased linearly with increasing length of nanowire. The slope of this graph gives the resistance per unit length and by measuring the height and width of the nanowire from the AFM image, the nanowire conductivity is estimated as 0.37 ± 0.029 S cm^{-1}. The conductivity of bulk PIm was also measured as a pressed pellet (~3.8×10^{-4} S cm^{-1}) which is less than the reported value of 1.9×10^{-3} S cm^{-1}.[31] The conductivity of the nanowire is subject to some uncertainty owing to variations in diameter. Nevertheless, the measured conductivity of the PIm/DNA nanowire is clearly substantially greater than the bulk conductivity. Similar observations have also been made for other conductive polymers such as polyindole.[18] However, the conductivity of the PIm/DNA nanowires is at least an order of magnitude smaller than the reported conductivity of PPy/DNA nanowires[16] (4 S cm^{-1}) and PIn/DNA nanowires (2.5 - 40 S cm^{-1}).[18] It is worth emphasizing that these values are not subject to errors due to contact resistance because that affects

the intercept rather than the slope of the plots in Fig. 8. The large (millimetre scale) contact between the eutectic and the nanowires typically has negligible resistance[51] in the range 50-200 Ω and therefore, the most significant source of contact resistance is the tip/nanowire contact because it has the smallest cross section. Fig. 8a illustrates the effect of increasing the tip/nanowire contact force by increasing the AFM set point voltage from 0 to 2 V. A clear decrease in the intercept on the resistance axis is observed at higher forces, but the slopes of the plots are unchanged within the uncertainty.

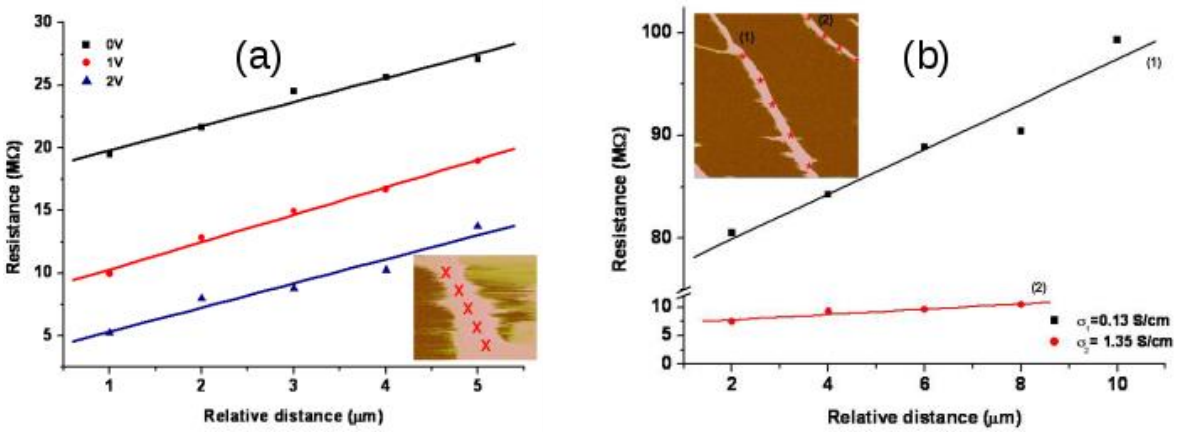

Figure 8: **(a)** PIm/DNA nanowire resistance at zero bias as a function of tip-contact relative distance for different applied forces in single-point c-AFM *I-V* measurements. The inset shows the current map of a nanowire of diameter 30 nm and length 5 μm. The current sensitivity was 100nA, the applied bias was 1V and several *I-V* measurement positions are indicated by red crosses. **(b)** Pd/PIm/DNA nanowires resistance at zero bias as a function of tip-contact relative distance for different applied forces in single-point c-AFM *I-V* measurements. The inset shows the current map of the nanowires; their diameters are (nw1: 50 nm and nw2: 45 nm) respectively. The current sensitivity was 100 nA, the applied bias was 5V and several *I-V* measurement positions are indicated by red crosses.

The same procedures were used to measure the conductivity of the Pd/PIm/DNA nanowires (Fig. 8b). Although, the structural characterisation above shows the metallisation of the PIm/DNA by Pd, it was found that the conductivity of the Pd/PIm/DNA nanowires is of the same order as that of the PIm/DNA nanowires.

On the other hand, we found that the conductivity of the Pd/PIm/DNA nanowires (0.1-1.4 S cm^{-1}) is much lower than the conductivity of the Pd/DNA nanowires (1.6×10^4 S cm^{-1}).[27] These results suggest that in the case of Pd/PIm/DNA nanowires the current flows mainly through the polymer instead of between Pd nanoparticles and this may be explained by assuming that although the Pd is bound to the template, there are

gaps between adjacent Pd nanoparticles on the template (Scheme 3 below). C-AFM does not readily permit observation of the temperature dependence of the conductivity and therefore we carried out measurements on nanowire networks formed between microfabricated gold electrodes.

Electrical characterisation of nanowire networks using two-terminal I-V measurements on microfabricated electrodes

In order to measure the *I-V* curves as a function of temperature, Pd/PIm/DNA nanowires were deposited between gold microelectrodes using the same route employed for Pd/DNA nanowires.[27] It should be noted here that difficulties were faced in achieving good contact between the nanowires and the gold electrodes which made it difficult to measure the *I-V* curves for a single nanowire. For this reason, a network of nanowires (see AFM in supporting information) was prepared between two gold microelectrodes to enhance the contact between the nanowires and the contact pads. Such networks of nanowires are formed when the silanization of the SiO_2 is omitted.[27] Measurements were then performed in two-point geometry by sweeping the bias voltage applied to the network (from −0.5 to 0.5 V) and recording the current. Although a linear *I-V* characteristic has been observed in the case of Pd/DNA nanowire networks,[27] among all the Pd/PIm/DNA networks we measured, no simple linear I-V characteristics were observed. Instead, a 'diode-like' *I-V* characteristic was observed as shown in Fig. 9a over a range of temperatures from -40^{o}C to 100^{o}C. This suggests an asymmetric network-electrode contact barrier at each side of the network. Nevertheless, the conductance (G) of the network is extracted at zero bias from the slope of the curves at each measured temperature. A small hysteresis in the G versus T plot was observed upon heating and cooling cycles (supporting information), particularly at temperatures higher than room temperature.

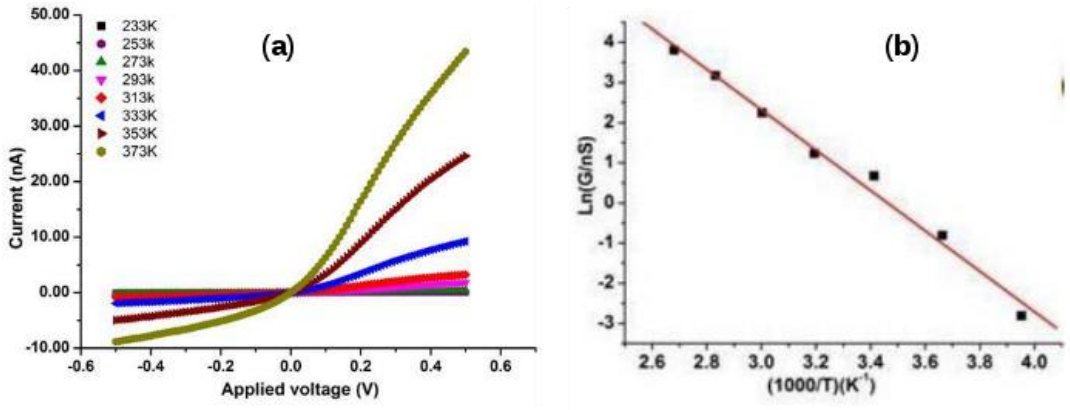

Figure 9: **(a)** Current voltage curves for the Pd/PIm/DNA nanowires network. Each curve was recorded at a fixed temperature and the full data set covers the temperature range of 233-373 K. **(b)** An Arrhenius plot for the zero-bias conductance of the network of Pd/PIm/DNA nanowires from the dataset in (a).

We found that the conductance of both Pd/DNA[31] and Pd/PIm/DNA nanowires is increased with increasing temperature which is a non-metallic electronic transport behaviour. However, this type of conduction behaviour has been previously observed in other metal nanowires such as platinum nanowires, fabricated using a focused ion beam method,[54] in which the resistance curves were fitted to a variable range hopping model. Lund and co-workers have also reported such negative thermal coefficients of resistivity for DNA-templated Pd nanowires.[55] In previous work we observed a temperature dependence of the Pd/DNA conductance that fitted a granular metal model:

$$\mathrm{G}=G_0 e^{-\left(\frac{T_0}{T}\right)^{\beta}} \qquad (1)$$

Where G is the conductance at temperature T and β = 0.5 for Pd/DNA.[27]

The corresponding Arrhenius plot of the conductance of the Pd/PIm/DNA network is shown in the Fig. 9b. It is clear that the Arrhenius equation (β = 1 in equation (1)) describes the conductance data over this temperature range and the fitted parameters are G_0 (0.036 S) and T_0 (5040 ± 245K) or in terms of energy, E_a (0.43 ± 0.02 eV).

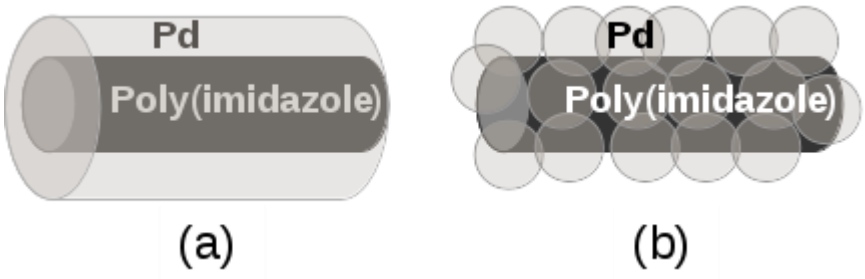

Scheme 3. Schematic diagram of the Pd/PIm/DNA nanowires. **(a)** the Pd shell is continuous and electrically conductive **(b)** the Pd coating is granular with poor electrical contact between Pd grains, but may nevertheless appear continuous in AFM image because of tip-radius limitations. The electrical data provides evidence that (b) is a better description of the Pd/PIm/DNA nanowires.

In summary, the magnitude of the conductivity of Pd/PIm/DNA nanowires is much less than that of Pd/DNA nanowires and comparable to PIm/DNA nanowires. The temperature dependence of their conductivity shows Arrhenius behaviour ($\beta = 1$) which we have found for other conductive polymer nanowires.[18] This is distinct from the behaviour of Pd/DNA nanowires whose conductance is not as strongly temperature-dependent ($\beta = 0.5$) and which may be described in terms of a granular metal model. We therefore conclude that the Pd/PIm/DNA nanowires comprise small Pd crystallites bound to PIm and decorating the nanowire, but not in good electrical contact with each other – illustrated in Scheme 3(b).

Conclusions

Hybrid Pd, polyimidazole nanowires (Pd/PIm/DNA) were fabricated by an electroless chemical method using PIm/DNA nanowires as a template. These were in turn formed by templating polyimidazole on DNA molecules. Structural and chemical characterisation demonstrates the formation of Pd on the nanowires, but electrical characterisation using different methods shows that Pd/PIm/DNA nanowires behave more like PIm/DNA than Pd templated directly on DNA (Pd/DNA).[27] Both PIm/DNA and Pd/PIm/DNA nanowires were confirmed to be conductive by scanned conductance microscopy and by c-AFM *I-V* curves at single nanowires and the conductivities were of similar magnitude. Two-terminal *I-V* measurements of Pd/PIm/DNA networks revealed a nonlinear characteristic; the temperature dependence of the differential conductance at zero bias showed Arrhenius (activated) behaviour, distinct from that reported for Pd/DNA,[27] but similar to previous reports for conductive polymers templated on DNA.[16-18] The measured conductivity of

Pd/PIm/DNA nanowires by means of c-AFM is 4 orders of magnitude smaller than their counterpart Pd/DNA nanowires, but of the same order as PIm/DNA. This may be explained by a structure in which there are gaps between the Pd crystallites which are bound to the PIm/DNA template and the current must flow through the polymer. It also demonstrates that large variations in the conductivity of templated-metal nanowires can occur when the underlying template is altered.

Acknowledgements

X-ray photoelectron spectra were obtained at the National EPSRC XPS User's Service (NEXUS) at Newcastle University, an EPSRC mid-range facility. This work was financially supported by One North East, EU-FP7 project LAMAND (Contract no. 245565) and EU ITN NANOEMBRACE (Contract no. 316751).

References

(1) C. Fang, Y. Fan, J. M. Kong, G. J. Zhang, L. Linn and S. Rafeah*, Sensors and Actuators B*, 2007, **126**, 684 - 690.
(2) M. Taniguchi and T. Kawai, *Physica E*, 2006, **33**, 1 - 12.
(3) E. Braun and K. Keren, *Adv. Phys.*, 2004, **53**, 441 - 496.
(4) R. M. Stoltenberg and A. T. Woolley *Biomedical Microdevices*, 2004, **6**, 105 - 111.
(5) A. Houlton, A. R. Pike, M. A. Galindo and B. R. Horrocks, *Chem. Commun.*, 2009, 1797 - 1806.
(6) E. Braun, Y. Eichen, U. Sivan and G. Ben-Yoseph, *Nature*, 1998, **391**, 775 - 778.
(7) J. Richter, R. Seidel, R. Kirsch, M. Mertig, W. Pompe, J. Plaschke and H. K. Schackert, *Adv. Mater.*, 2000, **12**, 507 - 510.
(8) L. Berti, A. Alessandrini and P. Facci, *J. Am. Chem. Soc.*, 2005, **127**, 11216 - 11217.
(9) C. F. Monson and A. T. Woolley, *Nano Lett.*, 2003, **3**, 359 - 363.
(10) J. Richter, M. Mertig, W. Pompe, I. Mönch and H. K. Schackert, *Appl. Phys. Lett.*, 2001, **78**, 536 - 538.
(11) S. M. D. Watson, N. G. Wright, B. R. Horrocks and A. Houlton, *Langmuir*, 2009, **26**, 2068 - 2075.
(12) L. Dong, T. Hollis, B. A. Connolly, N. G. Wright, B. R. Horrocks and A. Houlton, *Adv. Mater.*, 2007, **19**, 1748 - 1751.
(13) S. Kundu, H. Lee and H. Liang, *Inorg. Chem.*, 2008, **48**, 121 - 128.
(14) Y. Ma, J. Zhang, G. Zhang and H. He, *J. Am. Chem. Soc.*, 2004, **126**, 7097 – 7101.
(15) X. Li, M. Wan, X. Li and G. Zhao, *Polymer*, 2009, **50**, 4529 - 4534.
(16) L. Dong, T. Hollis, S. Fishwick, B. A. Connolly, N. G. Wright, B. R. Horrocks and A. Houlton, *Chem. Eur. J.*, 2007, **13**, 822 - 828.

(17) S. Pruneanu, S. A. F. Al.-Said, L. Dong, T. A. Hollis, M. A. Galindo, N. G. Wright, A. Houlton and B. R. Horrocks, *Adv. Funct. Mater.*, 2008, **18**, 2444 - 2454.
(18) R. Hassanien, M. Al-Hinai, S. A. F. Al-Said, R. Little, L. Šiller, N. G. Wright, A. Houlton and B. R. Horrocks, *ACS Nano*, 2010, **4**, 2149 - 2159.
(19) S. M. D. Watson, J. H. Hedley, M. A. Galindo, S. A. F. Al-Said, N. G. Wright, B. A. Connolly, B. R. Horrocks and A. Houlton, *Chem. Eur. J.*, 2012, **18**, 12008 - 12019.
(20) S. M. D. Watson, M. A. Galindo, B. R. Horrocks and A. Houlton, *J. Am. Chem. Soc.*, 2014, **36**, 6649 - 6655.
(21) S. A. F. Al-Said, R. Hassanien, J. Hannant, M. A. Galindo, S. Pruneanu, A. R. Pike, A. Houlton and B. R. Horrocks, *Electrochem. Commun.*, 2009, **11**, 550 - 553.
(22) J. Gu, S. Tanaka, Y. Otsuka, H. Tabata and T. Kawai, *Appl. Phys. Lett.*, 2002, **80**, 688 - 690.
(23) Y. Maeda, H. Tabata and T. Kawai, *Appl. Phys. Lett.*, 2001, **79**, 1181 - 1183.
(24) K. Tanaka and M. Shionoya, *J. Org. Chem.*, 1999, **64**, 5002 - 5003.
(25) K. Nguyen, M. Monteverde, A. Filoramo, L. Goux-Capes, S. Lyonnais, P. Jegou, P. Viel, M. Goffman and J.-P. Bourgoin, *Adv. Mater.*, 2008, **20**, 1099 - 1104.
(26) S. Kundu, K. Wang, D. Huitink and H. Liang, *Langmuir*, 2009, **25**, 10146 - 10152.
(27) M. N. Al-Hinai, R. Hassanien, N. G. Wright, A. B. Horsfall, A. Houlton and B.R. Horrocks, *Faraday Discuss.*, 2013, **164**, 71 - 91.
(28) E. B. Anderson and T. E. Long, *Polymer*, 2010, **51**, 2447 - 2454.
(29) J. Fernández-Bertrán, L. Castellanos-Serra, H. Yee-Madeira and E. Reguera, *J. Solid State Chem.*, 1999, **147**, 561 - 564.
(30) H. L. Wang, R. M. O'Malley and J. E. Fernandez, *Macromolecules*, 1994, **27**, 893 - 901.
(31) V. Raj, D. Madheswari and M. Mubarak Ali, *J. Appl. Polym. Sci.*, 2011, **119**, 2824 - 2833.
(32) H. Satoshi, U. Chigusa, E. Kazuo and H. Masahiko, *Adv. Synth. Catal.*, 2007, **349**, 833 - 835.
(33) V. Udayakumar, S. Alexander, V. Gayathri, Shivakumaraiah, K. R. Patil and B. Viswanathan, *J. Mol. Catal. A*, 2010, **317**, 111 - 117.
(34) D. Bensimon, A. J. Simon, V. Croquette and A. Bensimon, *Phys. Rev. Lett.*, 1995, **74**, 4754 - 4757.
(35) D. A. Shirley, *Phys. Rev. B*, 1972, **5**, 4709 - 4714.
(36) J. Sadlej, A. Jaworski and K. Miaskiewicz, *J. Mol. Struct.*, 1992, **274**, 247 - 257.
(37) D. Billaud, B. Humbert, L. Thevenot, P. Thomas and H. Talbi, *Spectrochimica Acta A*, 2003, **59**, 163 - 168.
(38) A. A. Ouameur and H. A. Tajmir-Riahi, *J. Biol. Chem.*, 2004, **279**, 42041 – 42054; S. Alex and P. Dupuis, *Inorg. Chim. Acta*, 1989, **157**, 271 – 281; G. I. Dovbeshko, N. Y. Gridina, E. B. Kruglova and O. P. Pashchuk, *Talanta*, 2000, **53**, 233 - 246.
(39) C.-Y. Lee, P. Gong, G. M. Harbers, D. W. Grainger, D. G. Castner, L. J. Gamble, *Anal. Chem.*, 2006, **78**, 3316 - 3325.
(40) H. Talbi, E. B. Maarouf, B. Humbert, M. Alnot, J. J. Ehrhardt, J. Ghanbaja and D. Billaud, *J. Phys. Chem. Solids* 1996, **57**, 1145 - 1151.

(41) J. G. Eaves, H. S. Munro and D. Parker, *Polym. Commun.*, 1987, **28**, 38 - 40.
(42) H. Kim, E. S. Daniels, V. L. Dimonie and A. Klein, *J. Appl. Polym. Sci.*, 2009, **112**, 843 - 849.
(43) F. Yang, S.-C. Kung, M. Cheng, J. C. Hemminger and R. M. Penner, *ACS Nano*, 2010, **4**, 5233 - 5244.
(44) R. Díaz-Ayala, L. Arroyo, R. Raptis and C. R. Cabrera, *Langmuir*, 2004, **20**, 8329 - 8235.
(45) I. Stará, S. Zuber, B. Gruzza and V. Matolín, *Vacuum*, 1998, **50**, 89 - 91.
(46) T. W. Orent and S. D. Bader, *Surf. Sci.*, 1982, **115**, 323 - 334.
(47) F. Moreno-Herrero, J. Colchero and A. M. Baró, *Ultramicroscopy*, 2003, **96**, 167 - 174.
(48) Mariam Al-Hinai, PhD thesis, Newcastle University, UK, 2012, pp141-142.
(49) S. M. D. Watson, A. R. Pike, J. Pate, A. Houlton and B. R. Horrocks, *Nanoscale*, 2014, **6**, 4027 - 4037.
(50) C. Staii, A. T. Johnson and N. J. Pinto, *Nano Lett.*, 2004, **4**, 859 - 862.
(51) R. Hassanien, S. A. F. Al-Said, L. Šiller, R. Little, N. G. Wright, A. Houlton and B. R. Horrocks, *Nanotechnology*, 2012, **23**, 075601.
(52) Y. Zhou, M. Freitag, J. Hone, C. Staii, A. T. Johnson, N. J. Pinto and A. G. MacDiarmid, *Appl. Phys. Lett.*, 2003, **83**, 3800 - 3802.
(53) M. Bockrath, N. Markovic, A. Shepard, M. Tinkham, L. Gurevich, L. P. Kouwenhoven, M. W. Wu and L. L. Sohn, *Nano Lett.*, 2002, **2**, 187 - 190.
(54) G. D. Marzi, D. Iacopino, A. J. Quinn and G. Redmond, *J. Appl. Phys.*, 2004, **96**, 3458 - 3462.
(55) J. Lund, J. Dong, Z. Deng, C. Mao and B. A. Parviz, *Nanotechnology*, 2006, **17**, 2752 - 2757.

Supporting information for

Metal-conductive polymer hybrid nanostructures: preparation and electrical properties of palladium-polyimidazole nanowires

Mariam Al-Hinai[1], Reda Hassanien*[2], Scott M. D. Watson[3], Nicholas G. Wright,[4] Andrew Houlton[3] and Benjamin R Horrocks[3]

[1] College of Applied Sciences Sohar, Engineering Department, P.O. Box 135, P.C. 311, Oman

[2] Department of Chemistry, Faculty of Science, Assiut University, New Valley Branch, El-Kharja 72511, Egypt.

[3] Chemical Nanoscience Laboratory, School of Chemistry, Bedson Building, Newcastle University, NE1 7RU, UK

[4] School of Electrical and Electronic Engineering, Merz Court, Newcastle University, NE1 7RU, UK

1. UV-Vis absorption spectroscopy data
2. Additional FTIR spectroscopic data and table of assignments
3. X-ray photoelectron spectroscopy – survey spectrum
4. Electrode characterisation (AFM / optical)
5. AFM image of a nanowire network on the microfabricated electrodes and current-voltage data.

1. UV-Vis absorption spectroscopy.

Method

UV–vis absorbance spectra were recorded on a Thermo Spectronic GENESYS 6 spectrophotometer (wavelength range from 250–550 nm, cell pathlength 1 cm). For UV-Vis measurements, PIm/DNA solution was made using calf thymus DNA (CT-DNA) (330 ng μL^{-1}; 10 mM tris-HCl pH 8; 1 mM EDTA). Typically, 0.25 mL of 3 mM freshly prepared imidazole solution was added to 1 mL of an aqueous CT-DNA solution in the presence of 0.5 mM $MgCl_2$. Then, 0.25 mL of $FeCl_3$ (1 mM) was added drop-wise to the solution. The mixture was stirred and allowed to react at room temperature for 1h. PIm solutions were prepared by the same process, but without CT-DNA, and used as a control: the colour of the solution was observed to become light yellow upon addition of oxidant. Pd/PIm/DNA solution was prepared by adding 0.25 mL K_2PdCl_4 (3 mM) to the previously prepared PIm/DNA solution. After allowing the reaction mixture to react at room temperature for 10 min, 0.25 mL $NaBH_4$ solution (10 mM) was added to reduce the Pd(II) ions. The solution was thoroughly mixed and allowed to react for at least 1h at room temperature prior to measurements.

UV-Vis absorption spectroscopy

UV-Vis absorption spectroscopy was employed to monitor the templating of PIm on DNA and the subsequent deposition of Pd. The electronic spectra of imidazole, PIm, CT-DNA, PIm/DNA and Pd/PIm/DNA recorded at room temperature in aqueous solution are shown in Fig. S1. The UV absorption spectrum of imidazole (curve B, Fig. S1) shows two small peaks in the range 260–280 nm which are assigned to a π–π^* transition and a larger band at 310 nm due to the n–π^* transition.[S1] Upon polymerization, the 310 nm band maximum moves to 295 nm, but there is a long tail, characteristic of extended conjugation in the polymer, extending into the visible region with shoulders at 375 nm, 425 nm and 480 nm (curve C, Fig. S1). Similar features were observed in the spectra of our previous report for polyindole/DNA nanowires.[S2] The Pd/PIm/DNA and PIm/DNA spectra are not simple superpositions of the PIm and DNA spectra as can be seen from the clear differences in the spectra near 300 nm. These observations support the conclusion that there is an intimate interaction between PIm and DNA, not a simple mixed solution.

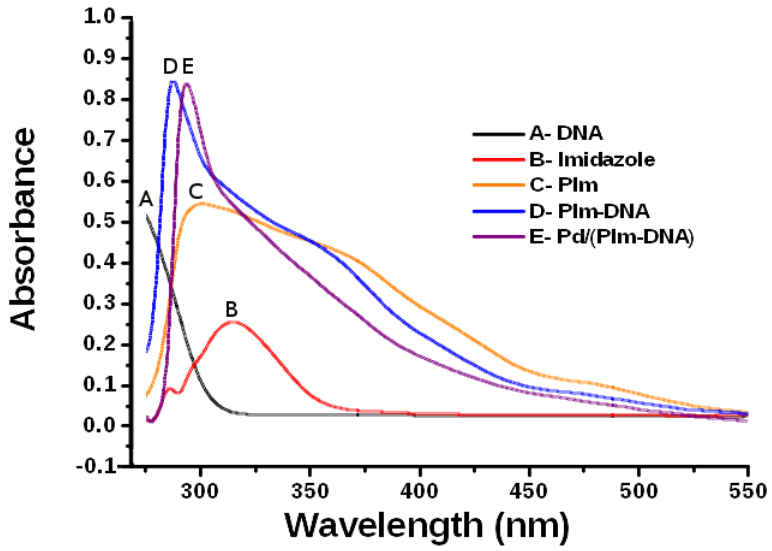

Figure S1. UV−Vis absorption spectra at different stages of the synthesis of Pd/PIm/DNA nanowires at room temperature. Absorption spectra of **(A)** DNA strands in water; **(B)** absorption spectrum of aqueous imidazole solution; **(C)** PIm solution prepared without DNA; **(D)** PIm/DNA solution and **(E)** Pd/PIm/DNA after addition of K_2PdCl_4 and $NaBH_4$ reduction. Concentration of stock CT-DNA solution: 330 ng μL^{-1}.

No distinctive surface plasmon resonance peak is observed in the Pd/PIm/DNA spectrum (curve E, Fig. S1). A broad absorption in the 300-550 nm region is typical for Pd nanostructures.[S3,S4] We have reported similar behaviour in Pd nanowires templated directly on DNA.[S5] In the case of Pd/PIm/DNA the plasmon is indistinguishable from the polymer absorption bands. UV-Vis spectroscopy therefore cannot confirm the metallisation and photoemission spectroscopy was required for this purpose.

References

(S1) T. Dhanalakshmi, E. Suresh, M. Palaniandavar, *Dalton Trans.*, 2009, 8317 - 8328.

(S2) R. Hassanien, M. Al-Hinai, S. A. F. Al-Said, R. Little, L. Šiller, N. G. Wright, A. Houlton and B. R. Horrocks, *ACS Nano*, 2010, **4**, 2149 - 2159.

(S3) S. Kundu, K. Wang, D. Huitink and H. Liang, *Langmuir*, 2009, **25**, 10146 - 10152.

(S4) J. A. Creighton and D. G. Eadon, *J. Chem. Soc., Faraday Trans.*, 1991, **87**, 3881 - 3891.

(S5) M. N. Al-Hinai, R. Hassanien, N. G. Wright, A. B. Horsfall, A. Houlton and B.R. Horrocks, *Faraday Discuss.*, 2013, **164**, 71 - 91.

2. Additional FTIR spectroscopic data

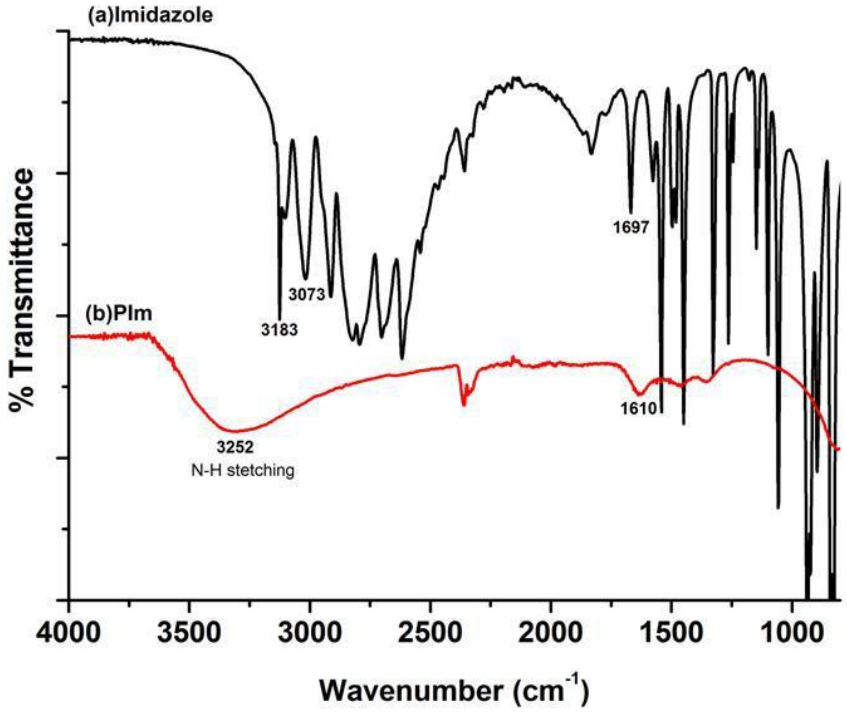

Figure S2 : FTIR spectra (KBr pellet) of (a) imidazole monomer (b) PIm product obtained by oxidation using $FeCl_3$.

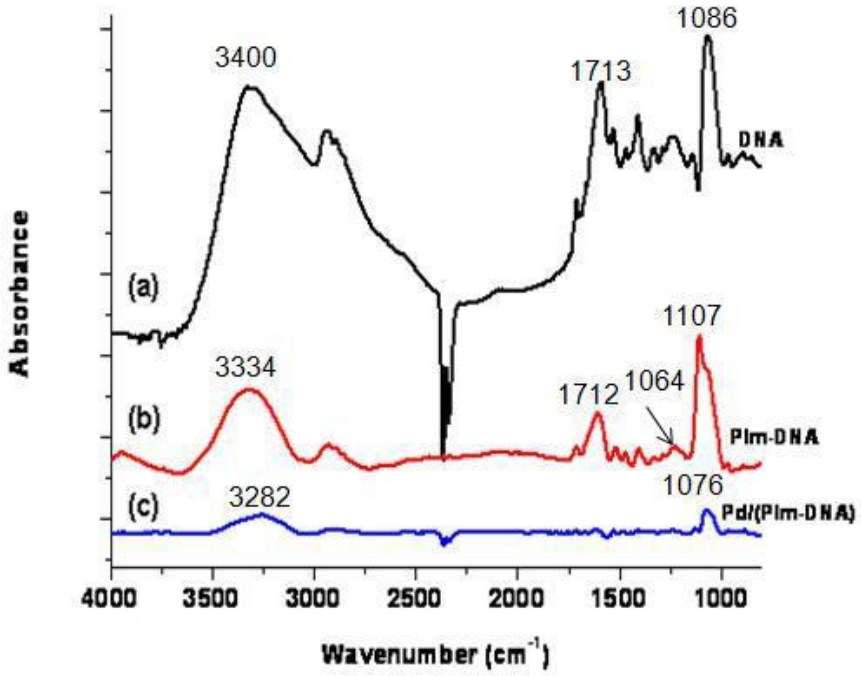

Figure S3 : FTIR spectra of (a) DNA (b) PIm/DNA and (c) Pd on PIm/DNA in the 4000-800 cm^{-1} region. The negative feature at 2360 cm^{-1} is CO_2 miscancellation.

Table S1. The main bands observed in the FTIR spectra of DNA, PIm/DNA and Pd/PIm/DNA in the 1800-800 cm^{-1} region. Spectral assignments from Refs S6-S8 below.

DNA	**PIm/DNA**	**Pd/PIm/DNA**	**Assignment**
891	893	887	C-H out-of-plane ring deformation (sugar-phosphate stretch)
964	968	972	C-O deoxyribose, C-C
1086	1107 1064	1076	PO_2^- symmetric stretch, deoxyribose-phosphate
1132	1193	1132	sym C–O–P stretching vibration
1219	1230	1242	PO_2^- asymmetric stretch, deoxyribose-phosphate
1286	1290	1307	Guanine, thymine, cytosine, adenine
1330	1332	1338	C-N stretch, thymine, adenine
1408	1408	1413	C-H, N-H deformation, C-N stretch (base-sugar moieties)
1468	1471	1485	C8-N coupled with a ring vibration of guanine
1529	1523	1533	in-plane vibration of cytosine and guanine
1598	1610	1612	C-N stretch, Adenine (C=N stretch of the guanine)
1713	1712	1724	Carbonyl stretches - the broad features in this region also include contributions from bound water molecules

(S6) A. A. Ouameur and H. A. Tajmir-Riahi, *J. Biol. Chem.*, 2004, **279**, 42041 – 42054.

(S7) S. Alex and P. Dupuis, *Inorg. Chim. Acta*, 1989, **157**, 271 – 281.

(S8) G. I. Dovbeshko, N. Y. Gridina, E. B. Kruglova and O. P. Pashchuk, *Talanta*, 2000, **53**, 233 - 246.

3. X-ray photoelectron spectroscopy – survey spectrum

The XPS overall survey spectrum of Pd on PIm/DNA sample

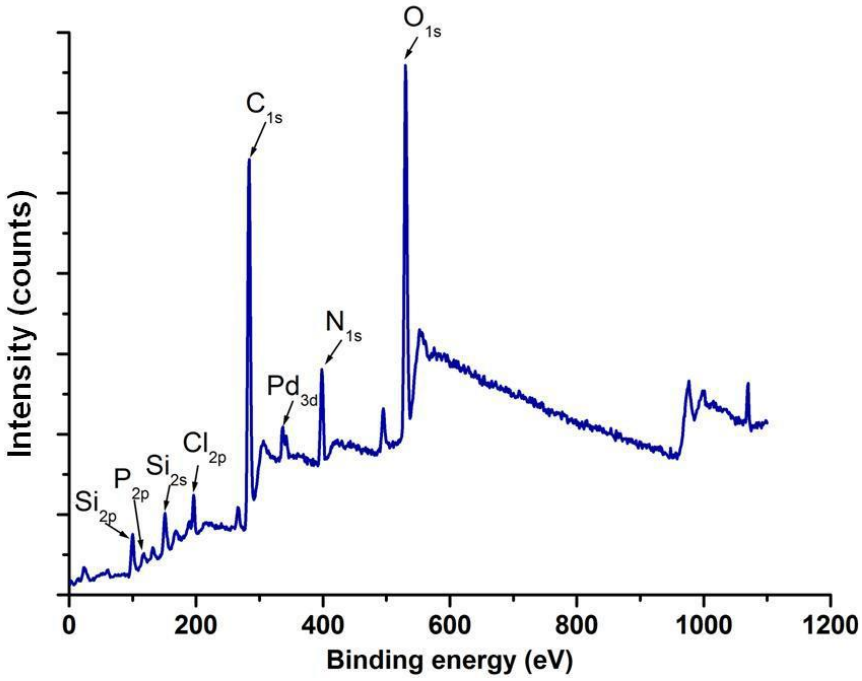

Figure S4 : XPS survey spectrum of the Pd on PIm/DNA nanowires.

4. Electrode characterisation (AFM / optical)

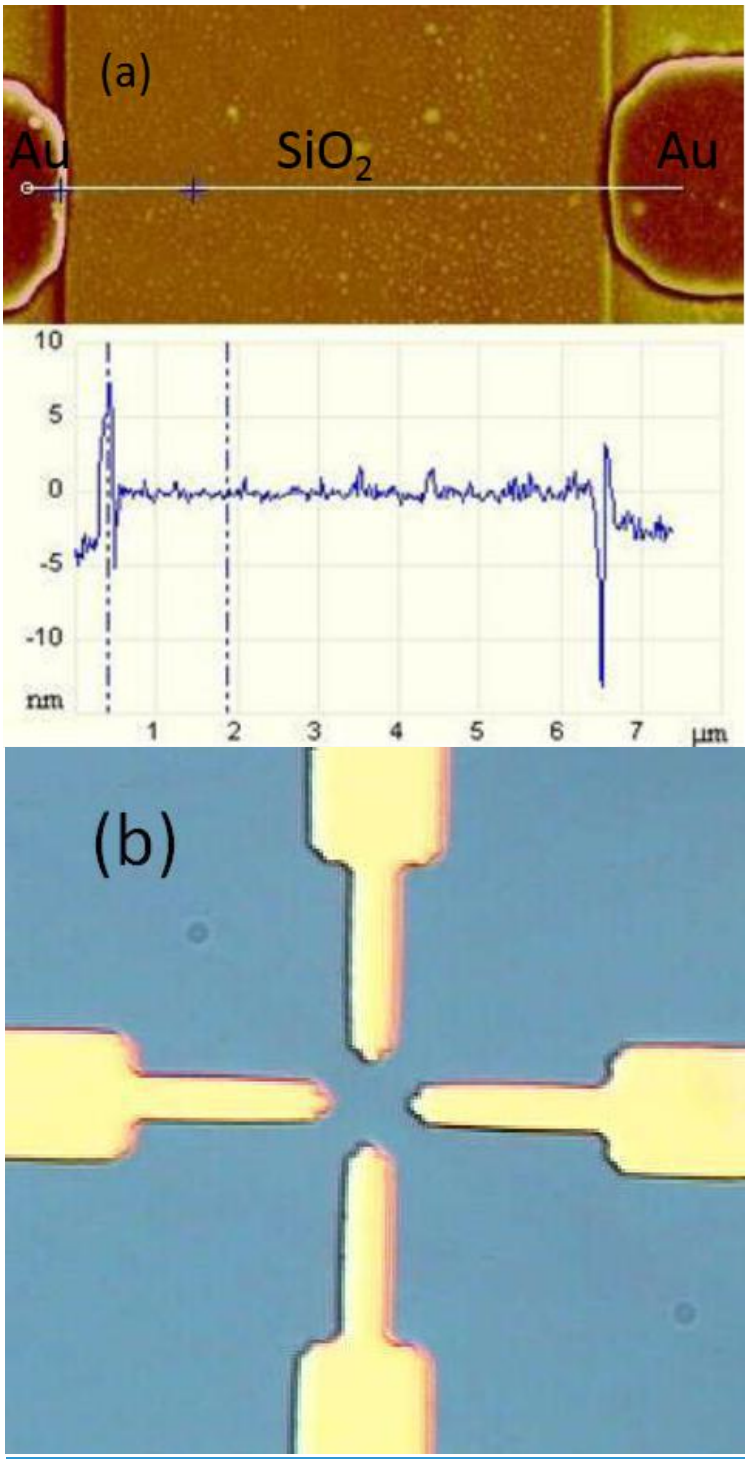

Figure S5 : (a) AFM characterisation of the step height at Au electrode – SiO_2 boundary. (b) Optical image of a set of four crossed electrodes as used for the current-voltage characterisation of nanowire networks.

5. AFM image of a nanowire network on the microfabricated electrodes and current-voltage data.

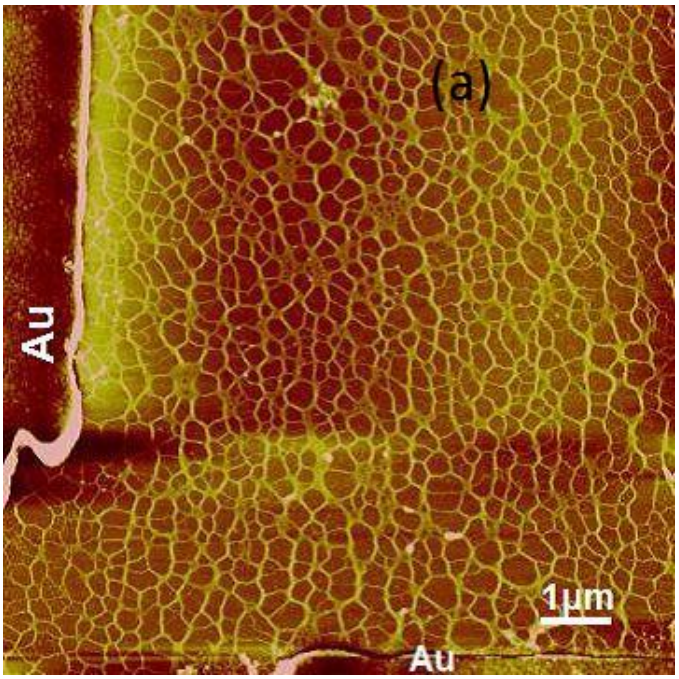

Figure S6a : AFM image of a Pd on PIm/DNA nanowire network between gold microelectrodes (the data scale is 25 nm) used to obtain the two terminal I-V measurements.

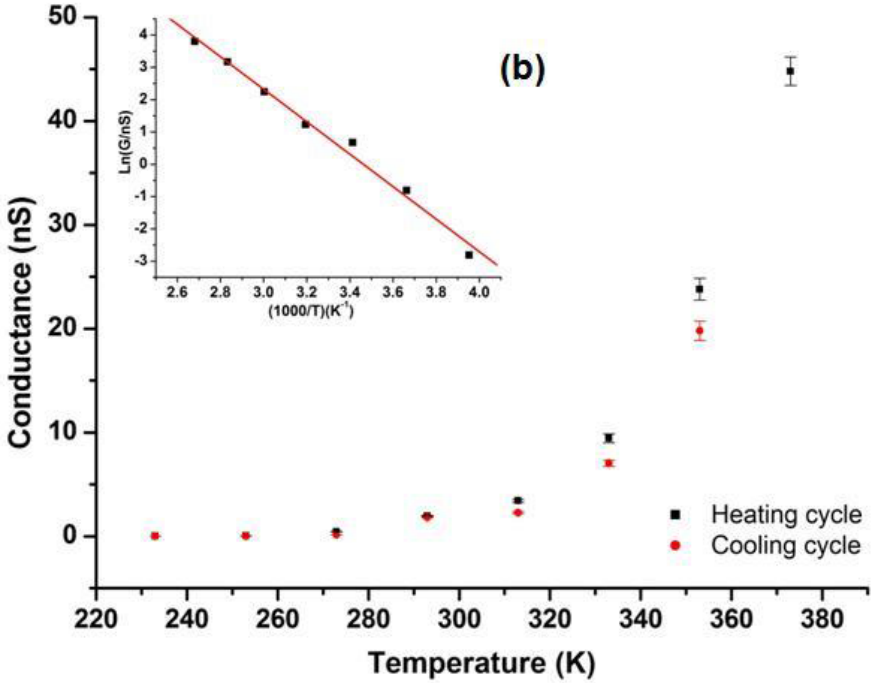

Figure S6b : Conductance vs. temperature for the data in (a), Inset is Arrhenius plot for the zero-bias conductance of the PIm/DNA/Pd network of nanowires.